PROCEEDINGS OF SPIE

SPIEDigitalLibrary.org/conference-proceedings-of-spie

# Imaging complex objects using learning tomography

JooWon Lim, Alexandre Goy, Morteza Hasani Shoreh , Michael Unser, Demetri Psaltis

JooWon Lim, Alexandre Goy, Morteza Hasani Shoreh , Michael Unser, Demetri Psaltis, "Imaging complex objects using learning tomography," Proc. SPIE 10503, Quantitative Phase Imaging IV, 105031T (23 February 2018); doi: 10.1117/12.2288920

SPIE.

Event: SPIE BiOS, 2018, San Francisco, California, United States

# Imaging complex objects using learning tomography

JooWon Lim[a], Alexandre Goy[a], Morteza Hasani Shoreh[a], Michael Unser[b] and Demetri Psaltis[a]

[a]Optics Laboratory, École Polytechnique Fédérale de Lausanne (EPFL), 1015 Lausanne, Switzerland

[b]Biomedical Imaging Group, École Polytechnique Fédérale de Lausanne (EPFL), 1015 Lausanne, Switzerland

## ABSTRACT

Optical diffraction tomography (ODT) can be described using the scattering process through an inhomogeneous media. An inherent nonlinearity exists relating the scattering medium and the scattered field due to multiple scattering. Multiple scattering is often assumed to be negligible in weakly scattering media. This assumption becomes invalid as the sample gets more complex resulting in distorted image reconstructions. This issue becomes very critical when we image a complex sample. Multiple scattering can be simulated using the beam propagation method (BPM) as the forward model of ODT combined with an iterative reconstruction scheme. The iterative error reduction scheme and the multi-layer structure of BPM are similar to neural networks. Therefore we refer to our imaging method as learning tomography (LT). To fairly assess the performance of LT in imaging complex samples, we compared LT with the conventional iterative linear scheme using Mie theory which provides the ground truth. We also demonstrate the capacity of LT to image complex samples using experimental data of a biological cell.

**Keywords:** Optical tomography, Mie scattering, Nonlinear optics

## 1. INTRODUCTION

The accurate modeling of the physics that govern the light scattering process is crucial in modern optical imaging modalities, especially in 3-D imaging. Recently, machine learning (ML) has received a lot of attention for post-processing of images for classification and segmentation outperforming conventional algorithms which are explicitly designed by humans. Therefore, it has motivated us to apply ML not only in post processing but also in modeling the underlying physics of the imaging system.[1]

Specifically we explore in this paper optical diffraction tomography (ODT). ODT is a powerful tool for imaging the 3-D refractive index (RI) distribution providing useful information such as cell structure and quantification of specific molecules.[2,3] However, there are open problems to be resolved. First of all, ODT is generally an ill posed problem because of the limited numerical aperture meaning that we can only acquire partial data. This missing cone problem causes the underestimation of RI values and distorts RI tomograms along the optical axis. More importantly, there exists an inherent nonlinearity. Conventionally, multiple scattering is neglected and reconstruction methods based on single scattering are used (Born and Rytov approximations). However, with the increase of complexity of sample, the single scattering approximations break down.[4,5] Especially, when there are multiple objects, even if each object is a week scatterer, multiple scattering among them makes the single scattering assumption invalid.[6]

To resolve those issues, there has been recently proposed many approaches.[7–13] We have focused on LT, a machine learning approach for ODT.[8,14] In the present contribution, we show the capacity of LT in imaging complex objects consisting of multiple cylinders using the analytical solution provided by generalized multiparticle Mie (GMM) theory,[15] which serves as the ground truth. More importantly, we confirm it by applying LT on real experimental data.

Further author information: (Send correspondence to JooWon Lim.)
JooWon Lim.: E-mail: joowon.lim@epfl.ch

Quantitative Phase Imaging IV, edited by Gabriel Popescu, YongKeun Park,
Proc. of SPIE Vol. 10503, 105031T · © 2018 SPIE · CCC code:
1605-7422/18/$18 · doi: 10.1117/12.2288920

## 2. THEORY

### 2.1 Optical diffraction tomography

The scattering in an inhomogeneous medium is governed by the Helmholtz equation,

$$\nabla^2 U_s(\mathbf{r}) + k^2 U_s(\mathbf{r}) = -4\pi F(\mathbf{r}) U(\mathbf{r}), \tag{1}$$

$U(\mathbf{r})$ is the total electric field which is the sum of the incident field, $U_i(\mathbf{r})$, and the scattered field, $U_s(\mathbf{r})$. The difference between the RI of the sample and the medium, $\Delta n(\mathbf{r}) = n(\mathbf{r}) - n_0$ generates the scattering potential, $F(\mathbf{r}) = \frac{k^2}{4\pi}\left(\frac{n(\mathbf{r})^2}{n_0^2} - 1\right)$. The optical wavelength in free space is $\lambda$ resulting in wavenumber, $k = \frac{2\pi n_0}{\lambda}$ . The integral solution of Eq. (1) can be obtained using the homogeneous Green's function resulting in

$$U_s(\mathbf{r}) = \int_V F(\mathbf{r}')U(\mathbf{r}')G(\mathbf{r}-\mathbf{r}')d\mathbf{r}', \tag{2}$$

where $G(\mathbf{r}-\mathbf{r}') = \frac{e^{ik|\mathbf{r}-\mathbf{r}'|}}{|\mathbf{r}-\mathbf{r}'|}$ is the Green's function of the 3-D Helmholtz equation, Eq. 1. Conventionally, to make Eq. 1 linear, the total electric field is approximated to be equal to the incident field resulting in the first order Born approximation. We can further approximate it by simply replacing $U_s(\mathbf{r})$ with the first order Taylor expansion, $U_s(\mathbf{r}) = U_i(\mathbf{r})(\frac{U(\mathbf{r})}{U_i(\mathbf{r})} - 1) = U_i(\mathbf{r})(e^{log(\frac{U(\mathbf{r})}{U_i(\mathbf{r})})} - 1) \simeq U_i(\mathbf{r}) \log \frac{U(\mathbf{r})}{U_i(\mathbf{r})}$. It results in the first order Rytov approximation which has been widely used in the field,

$$U_i(\mathbf{r}) \log \frac{U(\mathbf{r})}{U_i(\mathbf{r})} = \int_V F(\mathbf{r}')U_i(\mathbf{r}')G(\mathbf{r}-\mathbf{r}')d\mathbf{r}'. \tag{3}$$

We usually calculate the left term of Eq. 3 at $z = 0$ which is usually set to the center of the sample.

### 2.2 Learning tomography

One of the successful learning algorithms is based on convolutional neural networks (CNN). In general, each layer of a CNN is represented as $x_{j+1} = D[L[x_j * h]]$ where h is the convolution kernel, $L$ is a nonlinear operator (ex. ReLU) and $D$ is the down sampling operator for input $x_j$ and output $x_{j+1}$. There has been a recent research on combining a physical system of optical microscopy with the structure of CNN.[16] It is also possible to draw an analogy between the BPM and CNN where $h$ is the fixed diffraction kernel and $L$ is the z-slice dependent refraction operator without any down sampling. BPM consists of two sub steps, diffraction followed by refraction. Given the envelope of the electric wave as $S(x, y, z)$ for $U(x, y, z) = S(x, y, z)e^{ikz}$, BPM can be written as

$$S(x, y, z + \Delta z) = R^z[S(x, y, z) * d(x, y)]. \tag{4}$$

$d(x, y) = \frac{1}{(2\pi)^2}\iint e^{-i(k_x^2+k_y^2)/(k-\sqrt{k^2-k_x^2-k_y^2})}dk_x dk_y$ is a 2-D diffraction kernel and $R^z[f(x, y)] = e^{ik_0\Delta n(x,y,z+\Delta z)\Delta z}f(x, y)$ is a 2-D refraction operator decided at z-th section where $k = \frac{2\pi n_0}{\lambda}$, $\Delta n$ is the contrast between RI of the sample, $n(x, y, z)$, and RI of the medium, $n_0$. We use the notation $\mathbf{r} = (x, y, z)$ and $\mathbf{k} = (k_x, k_y, k_z)$ for the spatial and frequency coordinates. Using the BPM as the forward model, we can define the cost function combined with a sparsity based regularization, TV, as follows,

$$C(\Delta n(x, y, z)) = \frac{1}{2L}\sum_{i=1}^{L} ||M^{(i)} - B^{(i)}(\Delta n(x, y, z))||_2^2 + \tau TV(\Delta n(x, y, z)), \tag{5}$$

where $B^i : \mathbb{R}^N \to \mathbb{C}^M$ represents the BPM with a certain i-th illumination, $M \in \mathbb{C}^M$ is the measurement at $z = K$ ($U(x, y, K)$ in this case) and $\tau$ is a regularization parameter. We minimize the cost function using a Fast Iterative Shrinkage-Thresholding Algorithm (FISTA) with stochastic gradient decent (SGD).[17] In this paper, in order to fairly compare the performance of the BPM, we also minimized the cost function using the single scattering propagation model using the Rytov approximation. This can be done by propagating using the right term of Eq. 3 in stead of the BPM. Then, we can use the propagated field of $U_i(\mathbf{r}) \log \frac{U(\mathbf{r})}{U_i(\mathbf{r})}$ to $z = K$ using the propagation kernel[18] as $M^{(i)}$ in Eq. 5 and it results in follows,

$$F^{-1}[F[U_i(\mathbf{r}; z=0)\log\frac{U(\mathbf{r}; z=0)}{U_i(\mathbf{r}; z=0)}]e^{ik_z K}] = \int_V F(\mathbf{r}')U_i(\mathbf{r}')G(\mathbf{r}; z=K-\mathbf{r}')d\mathbf{r}', \tag{6}$$

where $F$ and $F^{-1}$ represent 2-D Fourier and inverse Fourier transform respectively.

## 3. METHOD

### 3.1 Experimental setup

The experimental setup consists of a Mach-Zehnder interferometer. To record off-axis digital holograms, the signal and reference arm are recombined at an angle of 1.43 degrees before the detector. The light source is a continuous wave laser diode at 406 nm. The light was spatially filtered and collimated. The effective numerical aperture of the system is 1.3. The image of the spheres was projected on an S-CMOS camera (Andor Neo) with an effective magnification of 111. In this study, we considered a single yeast cell as the sample. The sample was immersed in water and illuminated with plane waves through the illumination objective at different incidence angles. This could be achieved by placing two galvo-mirrors (one for the X and the other one for the Y direction) in conjugate image planes of the sample. We acquired 160 views equally spaced on a circle in the k x,y plane at an angle of 42 degrees from the optical axis (effective angle on the sample).

### 3.2 Reconstruction setup

The computational space was sampled with step size ($\Delta$x = $\Delta$y = $\Delta$z) of 0.08 $\mu m$ (multiple cylinders) or 0.0856 $\mu m$ (yeast cell). We manually set the regularization parameter, $\tau$, by trial and error ($\tau$ = 0.1 for multiple cylinders, $1e-4$ for yeast cell). For both models, we reduced the step size after every iteration, $\gamma^{k+1} = 0.985\gamma^k$. The iteration numbers for TV and FISTA are 20 and 200, respectively. For both of propagation models, the stochastic gradient method was used with 8 randomly chosen angles out of the total recorded angles at each iteration. In each case, the reconstruction obtained with direct inverse scattering based on the first order Rytov approximation was used as the initial condition. PUMA algorithm was used to unwrap the phase.[19] The PUMA algorithm could not properly unwrap the phase for several projections and these phases were not used in the reconstruction to get rid of artifacts from phase unwrapping and directly compare propagation models.

## 4. RESULTS

### 4.1 Multiple cylinders

We acquired simulated measurements using Mie theory for a single cylinder which induces phase delay of $\pi$. The RI contrast of the cylinder can be referred to as $\Delta n_0$ (Fig. 1(a)). After that, we placed four equal cylinders whose RI contrasts are $\Delta n_0/2$ as in Fig. 1(b) so that the overall induced phase delay is similar with the single cylinder case. Then we acquired synthetic measurements using GMM.[15] By applying the same principle, a set of $N$ cylinders whose RI contrasts are $\Delta n_0/\sqrt{N}$ can be generated. Therefore, the structural complexity of the sample can be controlled and we can investigate the performance of the single scattering model and the multiple scattering model in capturing the structure of complex sample. Figure 1 tells us that both of the single scattering and multiple scattering model break with the increase of the complexity showing smearing between cylinders. However, the LT generally shows more identical cylinders. To numerically evaluate it, we used the metric defined as

$$Error(n_{recon}, n_{true}) = \frac{||n_{recon} - n_{true}||_2^2}{||n_{true} - n_0||_2^2}, \tag{7}$$

where $n_{recon}$ is the reconstruction result (RI) and $n_{true}$ is the ground truth (RI) used in the Mie simulation. By comparing the *Error* of two propagation models tell us how one model is better than the other and we call it *Relative Error*.

$$Relative\ Error(n_{sgl}, n_{mlp}, n_{true}) = \frac{Error(n_{sgl}, n_{true})}{Error(n_{mlp}, n_{true})}, \tag{8}$$

where $n_{sgl}$ and $n_{mlp}$ are solutions acquired from the single scattering and multiple scattering propagation models, respectively. Figure 2 (a) shows that the *Error* of LT is lower than the single scattering tomography. By

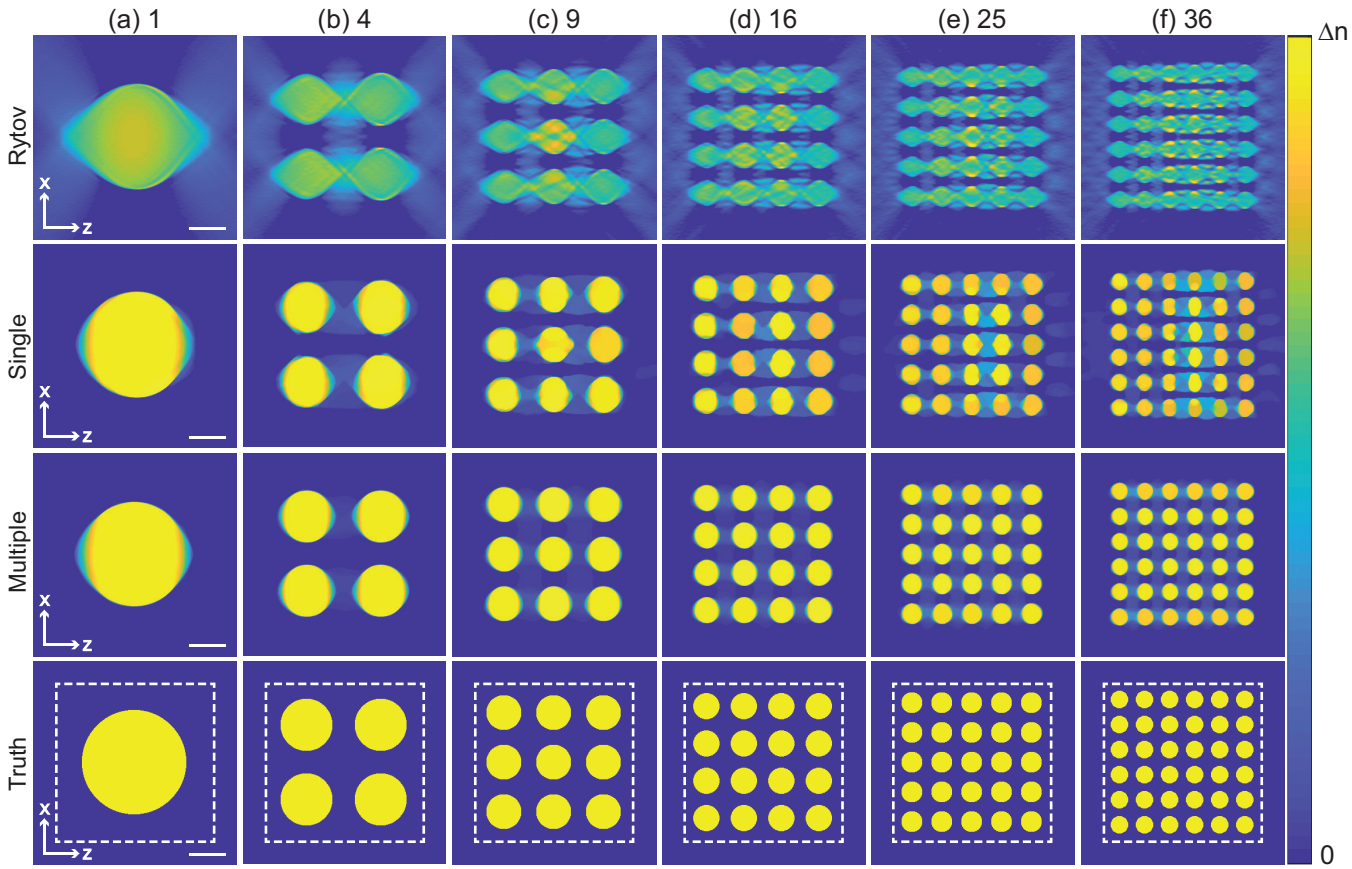


Figure 1. XZ cross sections of RI tomograms of multiple sets of multiple cylinders. From the left to the right, the RI contrast of each cylinder varies according to $\Delta n_0/\sqrt{N}$ where $\Delta n_0 = 0.0142$ and $N$ is the total number of cylinders in a set. From the first row to the fourth row, Rytov, single scattering, multiple scattering, and the ground truth. Scale bars are 5 $\mu m$.

comparing the *Error*s for the other cases, we get the *Relative Error*s as shown in 2 (b) showing values bigger than 1 for every case at the end of iteration cycle. In other words, the performance of LT is numerically confirmed over the single scattering tomography. The end points of the *Relative Error*s are plotted in Fig. 2 (c). In the plot, the graph shows increase followed by plateau then slight decrease with the increase of the complexity (number of cylinders). There is a certain range where the performance of LT gets maximized. This is because the BPM used in LT provides an inadequate estimate for the scattered field by the object due to the neglect of reflections and the vectorial nature of the optical field. However, we would like to stress that the LT still outperformed the single scattering tomography in the simulation meaning that the LT provides us a very powerful tool to image complex objects.

### 4.2 Single cell

A very important issue is whether the Mie theory results obtained for multiple cylinders tell us something about how well we can image a biological sample. There has been prior research on applying Mie theory on spheroidal scatterers such as cell nuclei in biological materials.[20] We can roughly think of cellular structures of a biological cell as aggregation of multiple spheres or cylinders. To test the capacity of the LT in imaging a complex sample, we reconstructed RI tomograms of a single yeast cell which has complex intracellular structures using the LT and compared it with images obtained with single scattering tomography. We concluded that the LT is more accurate in handling multiple scattering which dominates over the single scattering with the increase of complexity of sample. Figure 3 experimentally confirms this. Figure 3(b) clearly distinguish intracellular structures which are barely seen in Fig. 3(a) in the transverse ($xy$) plane. When it comes to the axial ($xz, yz$) planes, the effect gets

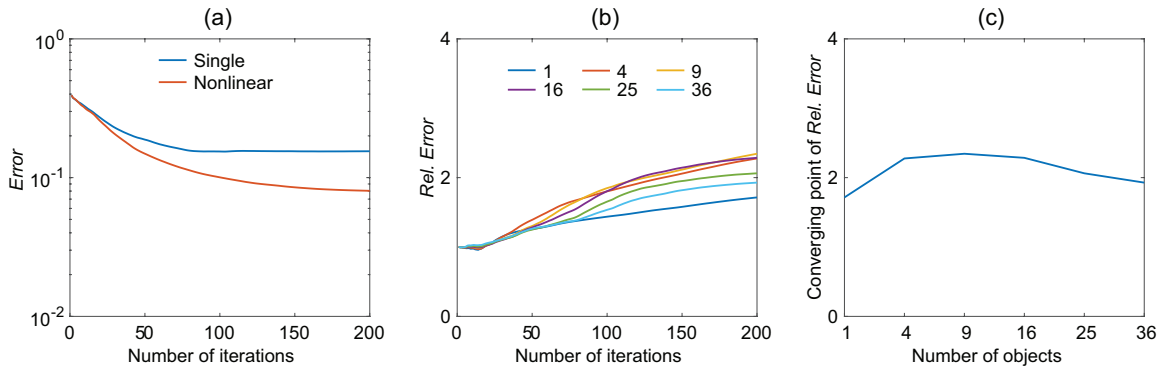


Figure 2. (a) *Error*s of the single scattering and multiple scattering models for a single cylinder. (b) *Relative Error*s for various sets of cylinders which differ in the complexity. (c) Converging points of *Error*s and *Relative Error*s.

pronounced and we attribute it to the fact that the LT handles multiple scattering in addition to the missing cone problem.

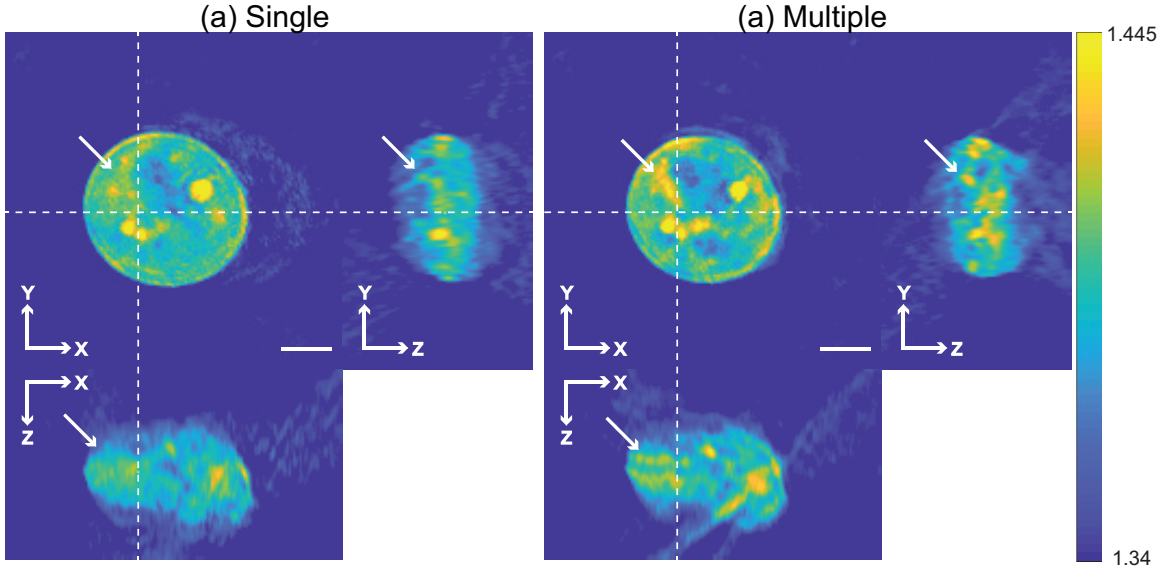


Figure 3. RI tomograms of a single yeast cell using two different propagation models (a) : single scattering, (b) : multiple scattering. Scale bars are 2 $\mu m$.

## 5. CONCLUSION

We demonstrated the superior performance of LT in imaging complex objects and compared it with the single scattering tomography. We acquired simulated measurements for multiple cylinders using GMM providing the ground truth. The number of cylinders were controlled to vary the degree of structural complexity of the object. It was shown that both models degrade with the increase in complexity but still the LT outperforms the single scattering tomography in each case. There is an intermediate level of sample complexity where the performance of LT gets maximized. In addition, we applied the LT to a single yeast cell which has intracellular structures. The results of the LT show clearly structures which are hard to observe using the conventional model.

## REFERENCES

1. Y. Rivenson, Y. Zhang, H. Gunaydin, D. Teng, and A. Ozcan, "Phase recovery and holographic image reconstruction using deep learning in neural networks," *arXiv preprint arXiv:1705.04286* , 2017.

2. W. Choi, C. Fang-Yen, K. Badizadegan, S. Oh, N. Lue, R. R. Dasari, and M. S. Feld, "Tomographic phase microscopy," *Nat. Methods* **4**(9), p. 717, 2007.
3. K. Lee, K. Kim, J. Jung, J. Heo, S. Cho, S. Lee, G. Chang, Y. Jo, H. Park, and Y. Park, "Quantitative phase imaging techniques for the study of cell pathophysiology: from principles to applications," *Sensors* **13**(4), pp. 4170–4191, 2013.
4. M. Slaney, A. C. Kak, and L. E. Larsen, "Limitations of imaging with first-order diffraction tomography," *IEEE Trans. Microw. Theory Techn.* **32**(8), pp. 860–874, 1984.
5. B. Chen and J. J. Stamnes, "Validity of diffraction tomography based on the first born and the first rytov approximations," *Appl. Opt.* **37**(14), pp. 2996–3006, 1998.
6. M. Azimi and A. Kak, "Distortion in diffraction tomography caused by multiple scattering," *IEEE Trans. Med. Imag.* **2**(4), pp. 176–195, 1983.
7. L. Tian and L. Waller, "3D intensity and phase imaging from light field measurements in an led array microscope," *Optica* **2**(2), pp. 104–111, 2015.
8. U. S. Kamilov, I. N. Papadopoulos, M. H. Shoreh, A. Goy, C. Vonesch, M. Unser, and D. Psaltis, "Learning approach to optical tomography," *Optica* **2**(6), pp. 517–522, 2015.
9. U. S. Kamilov, D. Liu, H. Mansour, and P. T. Boufounos, "A recursive born approach to nonlinear inverse scattering," *IEEE Signal Process. Lett.* **23**(8), pp. 1052–1056, 2016.
10. H.-Y. Liu, D. Liu, H. Mansour, P. T. Boufounos, L. Waller, and U. S. Kamilov, "Seagle: Sparsity-driven image reconstruction under multiple scattering," *arXiv preprint arXiv:1705.04281* , 2017.
11. E. Soubies, T.-A. Pham, and M. Unser, "Efficient inversion of multiple-scattering model for optical diffraction tomography," *Opt. Express* **25**(18), pp. 21786–21800, 2017.
12. J. Lim, A. Wahab, G. Park, K. Lee, Y. Park, and J. C. Ye, "Beyond born-rytov limit for super-resolution optical diffraction tomography," *Opt. Exp.* **25**(24), pp. 30445–30458, 2017.
13. J. Lim, A. Goy, M. H. Shoreh, M. Unser, and D. Psaltis, "Assessment of learning tomography using mie theory," *arXiv preprint arXiv:1705.10410* , 2017.
14. U. S. Kamilov, I. N. Papadopoulos, M. H. Shoreh, A. Goy, C. Vonesch, M. Unser, and D. Psaltis, "Optical tomographic image reconstruction based on beam propagation and sparse regularization," *IEEE Trans. Comput. Imag.* **2**(1), pp. 59–70, 2016.
15. J. Schäfer, S.-C. Lee, and A. Kienle, "Calculation of the near fields for the scattering of electromagnetic waves by multiple infinite cylinders at perpendicular incidence," *J. Quant. Spectrosc. Radiat. Transf.* **113**(16), pp. 2113–2123, 2012.
16. R. Horstmeyer, R. Y. Chen, B. Kappes, and B. Judkewitz, "Convolutional neural networks that teach microscopes how to image," *arXiv preprint arXiv:1709.07223* , 2017.
17. A. Beck and M. Teboulle, "A fast iterative shrinkage-thresholding algorithm for linear inverse problems," *SIAM. J. Imaging. Sci.* **2**(1), pp. 183–202, 2009.
18. W. Choi, C. Fang-Yen, K. Badizadegan, R. R. Dasari, and M. S. Feld, "Extended depth of focus in tomographic phase microscopy using a propagation algorithm," *Opt. Lett.* **33**(2), pp. 171–173, 2008.
19. J. M. Bioucas-Dias and G. Valadao, "Phase unwrapping via graph cuts," *IEEE Trans. Image Process.* **16**(3), pp. 698–709, 2007.
20. J. D. Keener, K. J. Chalut, J. W. Pyhtila, and A. Wax, "Application of mie theory to determine the structure of spheroidal scatterers in biological materials," *Opt. Lett.* **32**(10), pp. 1326–1328, 2007.